

BASIC RESEARCH PAPER

MIR506 induces autophagy-related cell death in pancreatic cancer cells by targeting the STAT3 pathway

Longhao Sun^{a,b,c}, Limei Hu^b, David Cogdell^b, Li Lu^c, Chao Gao^{a,b}, Weijun Tian^c, Zhixiang Zhang^c, Ya'an Kang^d, Jason B. Fleming^d, and Wei Zhang^{a,b}

^aDepartment of Cancer Biology, Comprehensive Cancer Center of Wake Forest Baptist Medical Center, Winston-Salem, NC, USA; ^bDepartment of Pathology, The University of Texas MD Anderson Cancer Center, Houston, TX, USA; ^cDepartment of General Surgery, Tianjin Medical University General Hospital, Tianjin, China; ^dDepartment of Surgical Oncology, The University of Texas MD Anderson Cancer Center, Houston, TX, USA

ABSTRACT

Pancreatic ductal adenocarcinoma (PDAC) is the most aggressive and lethal cancer. The role of autophagy in the pathobiology of PDAC is intricate, with opposing functions manifested in different cellular contexts. *MIR506* functions as a tumor suppressor in many cancer types through the regulation of multiple pathways. In this study, we hypothesized that *MIR506* exerted a tumor suppression function in PDAC by inducing autophagy-related cell death. Our results provided evidence that downregulation of *MIR506* expression was associated with disease progression in human PDAC. *MIR506* triggered autophagic flux in PDAC cells, which led to autophagy-related cell death through direct targeting of the *STAT3* (signal transducer and activator of transcription 3)-*BCL2-BECN1* axis. Silencing and inhibiting *STAT3* recapitulated the effects of *MIR506*, whereas forced expression of *STAT3* abrogated the effects of *MIR506*. We propose that the apoptosis-inhibitory protein *BCL2*, which also inhibits induction of autophagy by blocking *BECN1*, was inhibited by *MIR506* through targeting *STAT3*, thus augmenting *BECN1* and promoting autophagy-related cell death. Silencing *BECN1* and overexpression of *BCL2* abrogated the effects of *MIR506*. These findings expand the known mechanisms of *MIR506*-mediated tumor suppression to activation of autophagy-related cell death and suggest a strategy for using *MIR506* as an anti-*STAT3* approach to PDAC treatment.

ARTICLE HISTORY

Received 31 May 2016
Revised 18 December 2016
Accepted 30 December 2016

KEYWORDS

autophagy; autophagy-related cell death; *MIR506*; pancreatic ductal adenocarcinoma; *STAT3*

Introduction

Pancreatic ductal adenocarcinoma (PDAC) is considered the most lethal and aggressive of all neoplasms, with a dismal 5-y survival rate hovering around 6% and a median survival duration of less than 6 mo.^{1,2} Less than 15% of patients with PDAC are suitable for surgical resection because most have locally advanced or distant metastatic disease at the time of diagnosis.^{3,4} Even the most advanced chemotherapeutics and targeted therapies have brought only modest survival benefits.⁵ Thus, effective prognostic markers and novel treatment strategies and agents are urgently needed to improve the therapeutic outcome of PDAC.

Macroautophagy (referred to as autophagy) is an evolutionarily conserved cellular process that plays an important role in maintaining cellular homeostasis and overcoming metabolic stress and nutrient deprivation.^{6,7} Autophagy is observed in a wide range of cancer cells and its function varies significantly depending on cancer subtype and distinct cellular context. Under appropriate conditions, autophagy has cytoprotective roles and leads to therapeutic resistance by removing or mitigating harmful stimuli. Conversely, excessive or prolonged autophagy functions as a tumor-suppressive mechanism by


inducing autophagy-related cell death (type II programmed cell death or PCD) independent of, or in parallel with, apoptosis and necrosis in certain cellular conditions.^{8–11} Autophagy-related cell death can be induced by inhibition of anti-autophagic proteins in some apoptosis-resistant cancers, including PDAC.^{12–14} The role of autophagy in the pathobiology of PDAC is intricate, with opposing functions, but the mechanisms have not been well documented.¹⁵

STAT3 (signal transducer and activator of transcription 3) is a potent transcription factor that regulates the expression of more than 1,000 genes involved in multiple aspects of cellular processes.¹⁶ The prominent roles of *STAT3* in regulating autophagy are supported by growing evidence.^{17–22} *STAT3* functions as the main transcription regulator of several autophagy-related genes, such as *BCL2*, *BECN1*, *PIK3C3*, *PIK3R1*, *BNIP3*, and *HIF1A*. Because these genes function in a context-dependent manner, the crosstalk between autophagy and *STAT3* signaling may decide the survival or death of a cell.^{23–25}

MIR506, a component of an X chromosome-linked miRNA cluster, has been reported to function as an important tumor suppressor in many human cancers. Previous studies have

CONTACT Wei Zhang  wzhang@wakehealth.edu  Department of Cancer Biology, Comprehensive Cancer Center of Wake Forest Baptist Medical Center, 1 Medical Center Blvd., Winston-Salem, NC 27157, USA.

Color versions of one or more of the figures in the article can be found online at www.tandfonline.com/kaup

 Supplemental data for this article can be accessed on the publisher's website.

identified *MIR506* as a key gatekeeper for the network regulating epithelial-to-mesenchymal transition by regulating *SNAIL2*, *VIM*, and *CDH2*, and its expression is associated with good prognosis in ovarian and gastric cancers.^{26,27} *MIR506* suppresses proliferation and induces senescence by directly targeting the *CDK4-CDK6-FOXM1* axis.²⁸ The antiproliferative function of *MIR506* has also been established in esophageal, gastric, colorectal, and cervical cancers as well as glioblastoma and hepatocellular carcinoma.²⁹ *MIR506* is involved in the responses of ovarian cancers and pancreatic cancer to chemotherapy through regulation of *RAD51* and *SPHK1*.^{30,31} The role of *MIR506* in autophagic regulation, however, has not been reported.

Recent reports have shown that expression of *MIR506* is downregulated in PDAC tissues.^{31,32} Furthermore, *STAT3* was recently identified as a direct target of *MIR506*.³³ We hypothesized that *MIR506* exerted a tumor suppression function in PDAC by inducing autophagy-related cell death through targeting the *STAT3* pathway. In the current study, we investigated the expression of *MIR506* in different PDAC tissues and its relationship with the prognosis of the patients. Further experiments with patient-derived xenograft (PDX) cell systems revealed that *MIR506* functions as a tumor suppressor by inducing autophagy-related cell death through *STAT3* signaling pathways. Our findings have unveiled a previously unrecognized mechanism underlying the anticancer effects of *MIR506* against human PDAC.

Results

MIR506 downregulation is associated with disease progression in human PDAC

Quantification of *MIR506* expression in 92 matched pairs of human PDAC and adjacent normal tissues by quantitative reverse-transcriptase polymerase chain reaction (qRT-PCR) showed that the relative *MIR506* expression levels were significantly lower in PDAC tissues than in the adjacent normal tissues ($P < 0.01$; Fig. 1A). Clinicopathological analyses showed that lower *MIR506* expression in the tumors was significantly correlated with T status and TNM stage (TNM Classification of Malignant Tumors) (Table S1). The relative *MIR506* expression levels were significantly lower in the advanced tumor than early stage tumor (lower in the III-IV group and T3-T4 group than in the I-II group and T1-T2 group) ($P < 0.05$ and $P < 0.01$, respectively; Fig. 1B and C). Kaplan-Meier survival analysis indicated that patients whose tumor expressed a lower level of *MIR506* had a significantly lower overall survival rate (Fig. 1D).

MIR506 induces cell death in human PDAC cells

The effect of *MIR506* on proliferation of PDAC cells was evaluated by immunofluorescent staining for MKI67/Ki-67 in PDX lines MDA-PATC53, MDA-PATC124, and MDA-PATC148. *MIR506* dramatically decreased the MKI67-positive rate in PDAC cells (Fig. S1A). Consistent with this

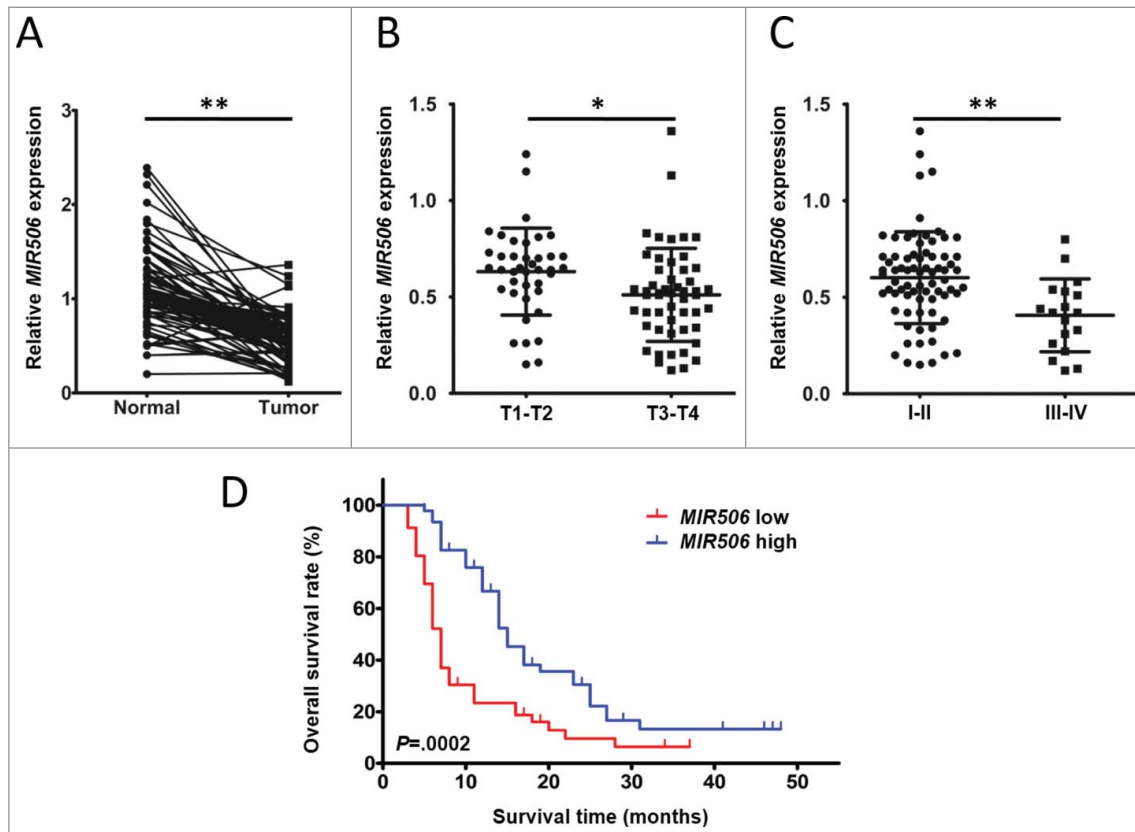


Figure 1. *MIR506* downregulation correlates with disease progression in human PDAC. (A) Comparison of *MIR506* expression in 92 matched pairs of PDAC tissues and corresponding nontumor tissues via qRT-PCR. *RNU6* was used as an internal control. (B) Comparison of *MIR506* expression in stage T1-T2 and stage T3-T4 PDAC tissues. (C) Comparison of *MIR506* expression in stage I-II and stage III-IV PDAC tissues. * $P < 0.05$; ** $P < 0.01$. (D) Kaplan-Meier curves compared the overall survival rates of PDAC patients whose tumor expressed a low or high level of *MIR506*. The median value was used as the cut-off point for definition of low and high *MIR506* expression groups.

finding was the observation that *MIR506* significantly impaired the colony-formation capacity of PDAC cells (Fig. S1B). Assessment of the cell cycle distribution of these cells by propidium iodide (PI) staining and bromodeoxyuridine (BrdU) assay demonstrated that all *MIR506*-transfected cells had a higher fraction in G₁ phase and a corresponding lower fraction in S phase than cells transfected with control miRNA (*MIRctrl*) (Fig. S2). Luciferase reporter assay showed that *MIR506* suppressed proliferation and induced G₁ arrest by directly targeting *CDK4-CDK6* (Fig. S3) in PDAC cells, which was similar to what we reported in ovarian cancer cells.

The 3-(4,5-dimethylthiazol-2-yl)-2,5-diphenyltetrazolium bromide (MTT) assay was performed to evaluate the impact of *MIR506* on PDAC cell viability. Surprisingly, cell viability significantly decreased in a time-dependent manner in *MIR506*-transfected PDAC cells (Fig. 2A), which contrasted with previous findings that *MIR506* resulted only in blockage of cell viability relative to that of control miRNA-treated cells.

We performed a trypan blue exclusion assay to confirm whether the *MIR506*-mediated decrease of PDAC cell viability was associated with cell death. The results show that *MIR506* induced cell death in a time-dependent manner (Fig. 2B). These results reveal that *MIR506* not only inhibited the proliferation of PDAC cells but also induced their death.

Cell death caused by *MIR506* is dependent on autophagy

To determine the mode of cell death caused by *MIR506*, we first investigated whether the cytotoxicity was related to apoptosis. PDAC cells treated with *MIR506* or the apoptosis inducer 5-fluorouracil (5-FU) were exposed to the selective inhibitor of apoptosis N-benzyloxycarbonyl-Val-Ala-Asp-fluoromethyl ketone (z-VAD-FMK). Cell death was analyzed by ANXA5-PI staining followed by flow cytometry. Z-VAD-FMK dramatically decreased the ANXA5-positive cell population induced by 5-FU but showed no effect on that induced by *MIR506* (Fig. 3A). The results of the trypan blue exclusion assay also showed that z-VAD-FMK significantly suppressed the apoptotic cell death caused by 5-FU but failed to protect the cells from death caused by *MIR506* (Fig. 3D). To confirm these results, we performed Apo-BrdU assays (to detect apoptotic cells) and immunoblotting. As shown in Figure 3G, *MIR506* failed to induce a significant increase in the Apo-BrdU-positive cell population. Consistent with this finding was the absence of cleaved CASP3 (caspase 3) and cleaved CASP9 in lysates of *MIR506*-transfected cells (Fig. 3H). These data show that *MIR506*, unlike 5-FU, induced predominantly non-apoptotic cell death.

To determine the role of necrosis in PDAC cell death, we pretreated cells with a selective inhibitor of necrosis, 2-(1H-Indol-3-yl)-3-pentylamino-maleimide (IM-54), to antagonize the cell death induced by *MIR506* or the known necrosis inducer tert-butyl hydroperoxide (t-BHP). IM-54 significantly

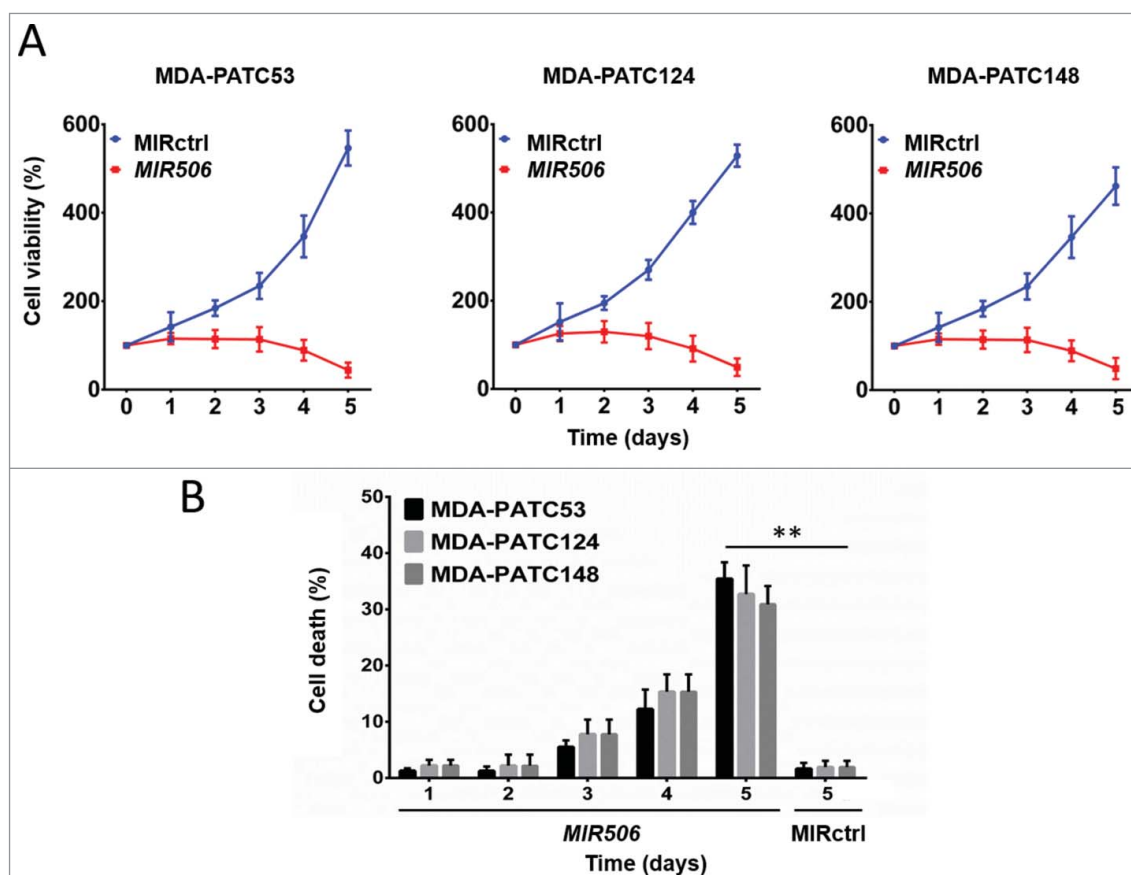


Figure 2. *MIR506* induces cell death in human PDAC cells. (A) MDA-PATC53, MDA-PATC124, and MDA-PATC148 cells were transfected with *MIRctrl* or *MIR506* for 5 d. Cell viability was measured by the MTT assay every day. (B) After transfection with *MIRctrl* or *MIR506*, cells were trypsinized and collected in PBS, and cell death was quantified by trypan blue exclusion assay every day. Data represent mean \pm SD of at least of 3 independent experiments. ** $P < 0.01$.

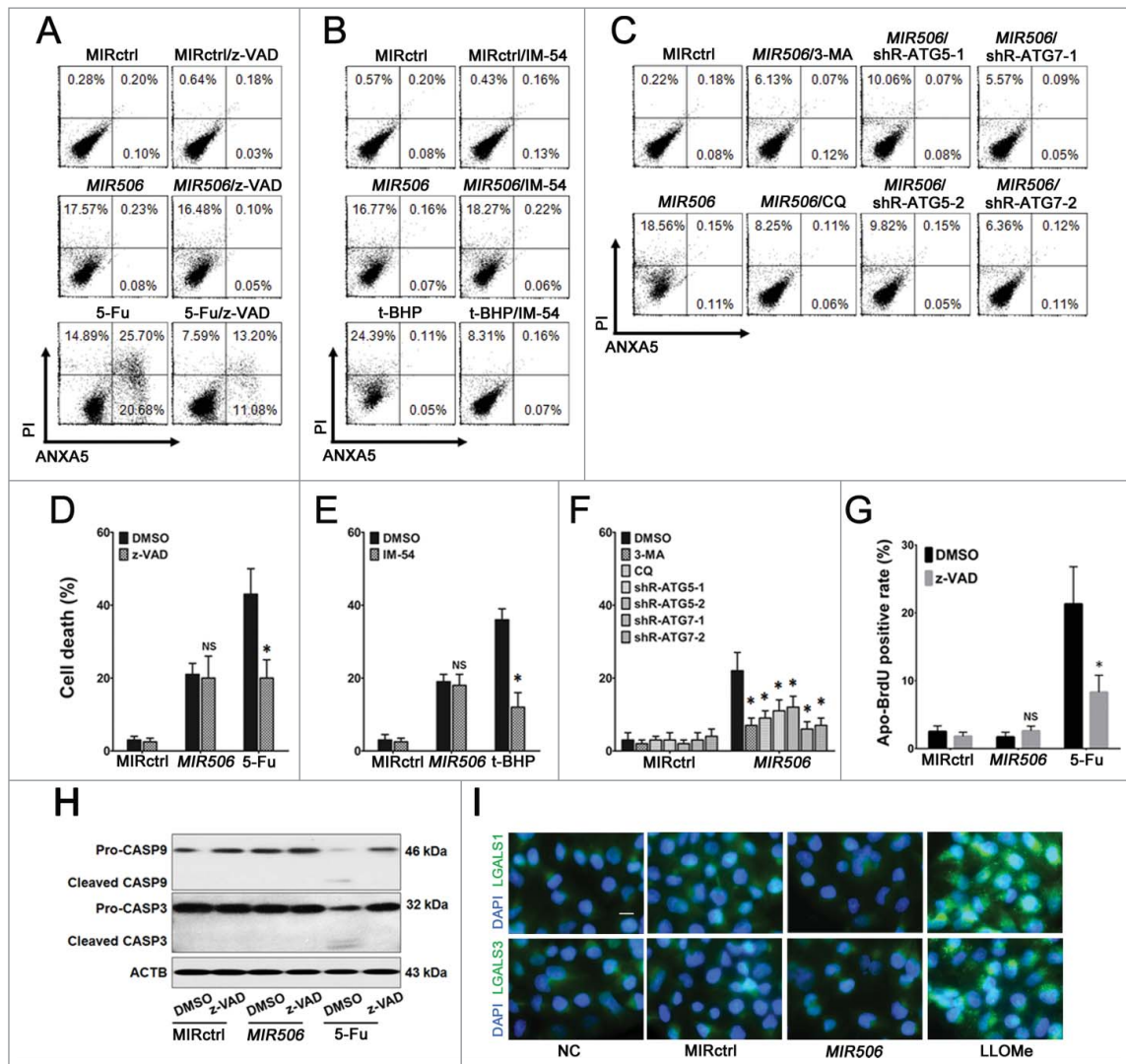


Figure 3. Cell death caused by *MIR506* is dependent on autophagy. (A) MDA-PATC53 cells were transfected with MIRctrl or *MIR506* or pretreated with apoptosis-inducer 5-FU in the absence (DMSO) or presence of the selective apoptosis inhibitor z-VAD-FMK (z-VAD; 20 mM) for 96 h; (B) MDA-PATC53 cells were transfected with MIRctrl or *MIR506* or pretreated with the necrosis promoter t-BHP in the absence (DMSO) or presence of necrosis inhibitor IM-54 (10 mM) for 96 h; (C) MDA-PATC53 cells were pretreated with the autophagy inhibitor 3-MA (5 mM) or CQ (50 μ M) or transfected with shRNAs to knock down *ATG5* or *ATG7* first, and then transfected with MIRctrl or *MIR506* for 96 h. Cells were trypsinized and analyzed by flow cytometry after being stained with FITC-labeled ANXA5-PI. (D-F) After pretreatment as described in (A-C), cell death was also quantified by trypan blue exclusion assay. (G) MDA-PATC53 cells were transfected with MIRctrl or *MIR506* or pretreated with 5-FU in the absence (DMSO) or presence of z-VAD-FMK (20 mM) for 96 h. Cells were labeled with Apo-BrdU and analyzed by flow cytometry. (H) After pretreatment as described in (G), whole-cell extracts of MDA-PATC53 cells were subjected to immunoblotting with anti-CASP3 and -CASP9 antibodies. (I) MDA-PATC53 cells were pretreated with or without the LMP inducer LLOMe (2 mM) or transfected with MIRctrl or *MIR506* for 96 h. Cells were fixed for immunofluorescent staining with anti-LGALS1 or -LGALS3 antibody and visualized with a fluorescence microscope. Data represent mean \pm SD of at least of 3 independent experiments. NS, not significant; * P < 0.05. Scale bar: 10 μ m.

reduced the ANXA5-negative, PI-positive cell population (Fig. 3B) and abrogated t-BHP-induced cell death (Fig. 3E), but it did not protect the cells from death and did not decrease the ANXA5-negative, PI-positive cell population induced by *MIR506*. These results show that necrosis was not the mode of *MIR506*-induced cell death.

To determine whether *MIR506*-induced cell death was associated with autophagy, we examined the effect of the autophagy inhibitors 3-methyladenine (3-MA) and chloroquine (CQ) in PDAC cells. Genetic inhibition of autophagy was also used to demonstrate the requirement of autophagy in the *MIR506*-induced cell death (Fig. S4). Pretreatment with 3-MA or CQ, or knockdown of the essential autophagy genes *ATG5* or *ATG7* by shRNA significantly prevented *MIR506*-induced cell death and caused a dramatic decrease

in the ANXA5-negative, PI-positive cell population in *MIR506*-treated cells (Fig. 3C and F). These results suggest that autophagy is the major mechanism of *MIR506*-induced cell death in PDAC cells.

Lysosomal membrane permeabilization (LMP) could be induced by a broad array of stimuli and leads to lysosomal cell death, which can present with apoptotic or necrotic features according to the extent of lysosomal hydrolase leakage. Because lysosomal cell death is often confused with autophagic cell death due to the accumulation of autophagosomes, we performed immunofluorescence by staining with LMP-specific markers LGALS1 and LGALS3 to rule out this possibility.³⁴ The LMP inducer L-leucyl-L-leucine methyl ester (LLOMe) was used as a positive control. The results showed that *MIR506* could not induce LMP (Fig. 3I).

MIR506 induces autophagic flux in PDAC cells

To confirm that *MIR506* can induce autophagy in PDAC cells, we performed an immunofluorescence analysis for LC3, a marker of autophagosome formation. The formation of LC3-labeled vacuoles was markedly increased in the cytoplasm after transfection with *MIR506* and could be prevented with 3-MA (Fig. 4A and B). We evaluated the formation of autolysosomes by flow cytometry after staining with acridine orange (AO). As shown in Fig. S5, *MIR506* significantly induced the formation of autolysosomes in PDAC cells, and the AO-positive cell population was reduced by the autophagy inhibitor 3-MA.

Autophagic flux was also monitored with the Premo Autophagy Tandem Sensor RFP-GFP-LC3. RFP fluorescence was detectable in both autophagosomes and autolysosomes, but GFP fluorescence was quenched in autolysosomes by the

low-pH environment. *MIR506* significantly increased the formation of autophagosomes and autolysosomes, indicating that it enhanced autophagic flux (Fig. 4C and D). Conversion of non-lipidated soluble LC3 (LC3-I) to phosphatidylethanolamine-conjugated LC3 (LC3-II) serves as a sensitive indicator of autophagy, and immunoblotting analysis revealed a dramatic increase in the ratios of LC3-II to LC3-I and LC3-II to actin in response to *MIR506* transfection. Our findings on the clearance of SQSTM1, another distinct feature of autophagy, were consistent with these results. To determine whether the observed high levels of autophagic markers were due to increased autophagic flux, we treated cells with the vacuolar-type H^+ -ATPase inhibitor bafilomycin A_1 (Baf-A), which prevents fusion between autophagosomes and lysosomes, thus inhibiting LC3 degradation.³⁵ Treatment with Baf-A caused significant increases of LC3-II accumulation in *MIR506*-transfected cells

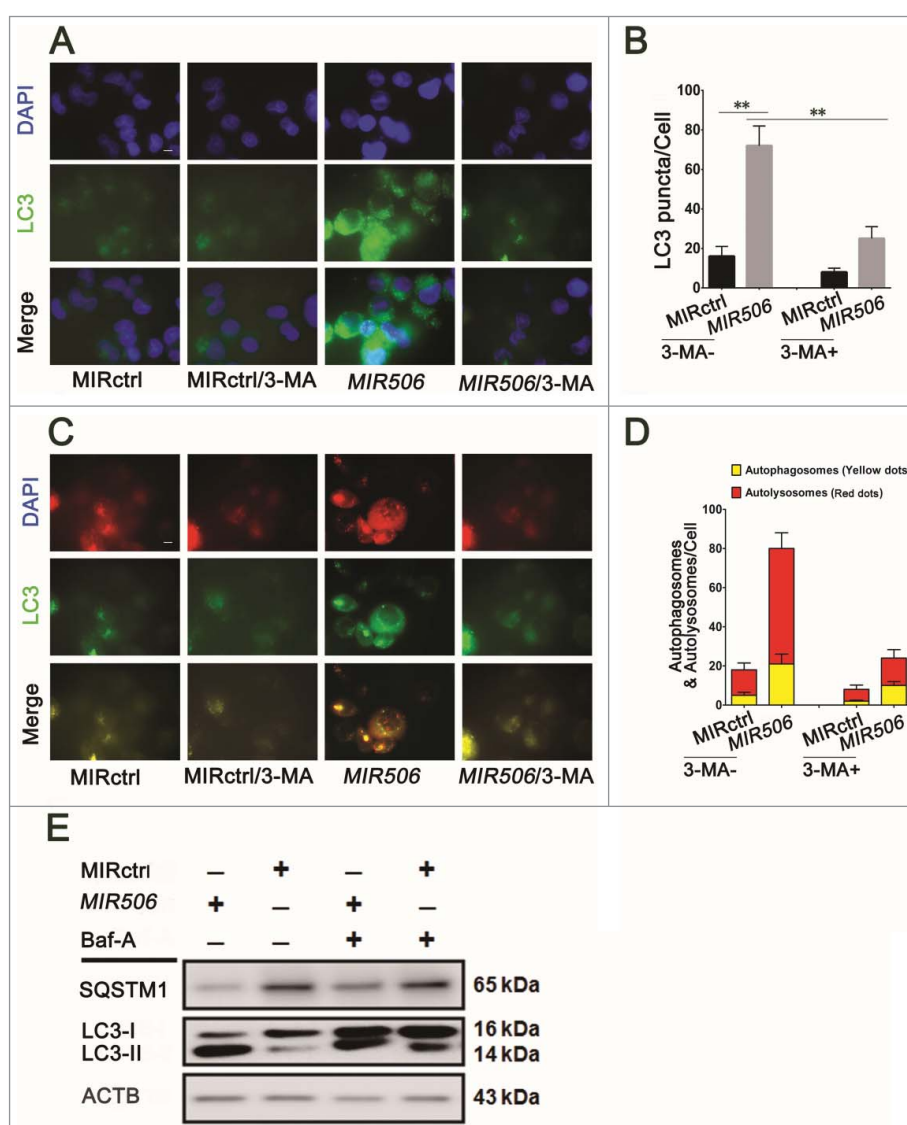


Figure 4. *MIR506* induces autophagic flux in PDAC cells. (A) MDA-PATC53 cells were transfected with MIRctrl or *MIR506* in the absence or presence of the autophagy inhibitor 3-MA (5 mM) for 72 h. Cells were fixed for immunofluorescent staining with anti-LC3 antibody and visualized with a fluorescence microscope. (B) The LC3 puncta in each cell were counted. $n = 100$ cells/sample, $**P < 0.01$. (C) MDA-PATC53 cells were transfected with MIRctrl or *MIR506* for 48 h and infected with Autophagy Tandem Sensor RFP-GFP-LC3 in the absence or presence of 3-MA (5 mM) for 24 h. Then, cells were visualized with a fluorescence microscope. (D) The autophagosomes (yellow dots) and autolysosomes (red-only dots) in each cell were counted. $n = 100$ cells/sample. (E) MDA-PATC53 cells were transfected with MIRctrl or *MIR506* in the absence or presence of the vacuolar-type H^+ -ATPase inhibitor Baf-A (10 nM). Whole-cell extracts were subjected to immunoblotting with anti-LC3 and -SQSTM1 antibodies. Scale bar: 10 μ m.

indicating that *MIR506* can enhance autophagic flux (Figs. 4E and S6). Taken together, these results support the idea that *MIR506* induced autophagic flux in PDAC cells.

MIR506 directly targets STAT3 and induces autophagy-related cell death in a STAT3-dependent manner

The miRNA target analysis algorithm TargetScan 6.0 predicted that the 3'-untranslated region (UTR) of *STAT3* mRNA contains a potential binding site of *MIR506* and this site is highly conserved among different species (Fig. 5A). We chose *STAT3* as a validation target because it is involved in multiple aspects of the autophagic process and was shown to be a direct target of *MIR506* in glioma cells in a recent report by Peng et al.³³ To examine the regulation of *STAT3* by *MIR506* we performed a luciferase reporter assay in MDA-PATC53 cells. Using a dual-luciferase reporter system, we showed that *MIR506* significantly inhibited the luciferase reporter activity of the wild-type but not the mutant *STAT3* 3'-UTR, indicating that *STAT3* is a direct target of *MIR506* in PDAC cells (Fig. 5B).

Immunoblotting and qRT-PCR analyses showed that *MIR506* significantly reduced the expression of *STAT3* at both protein and mRNA levels in all 5 PDAC cell lines tested (Fig. 5C-E). Marked conversion of LC3-I to LC3-II was detected only in cell lines with a high baseline level of *STAT3*, including MDA-PATC53, MDA-PATC124, and MDA-PATC148 (Fig. 5C). We also performed flow cytometry with AO staining to confirm the induction of autophagy. The results revealed that the AO-positive cell population increased significantly in response to *MIR506* only in cell lines with a high baseline *STAT3* level (Fig. S7). Consistent with these results, autophagy-related cell death was observed in cells with a high *STAT3* level but not in those with a low *STAT3* level (Fig. 5F). These results indicate that *MIR506* triggered autophagy-related cell death and that this effect was dependent on *STAT3*.

MIR506 induces autophagy-related cell death through the STAT3 signaling pathway

The *STAT3* signaling pathway, a prominent stress-responsive pathway, is involved in multiple aspects of the autophagic

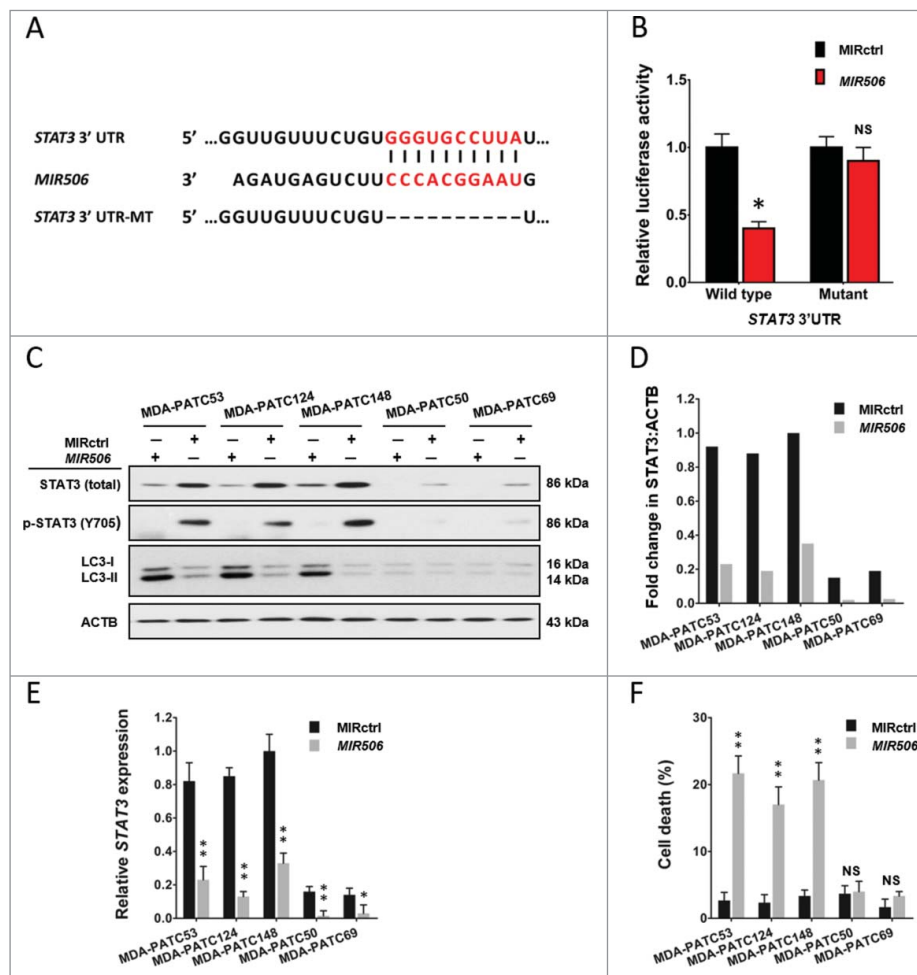


Figure 5. *MIR506* directly targets *STAT3* and induces autophagy-related cell death in a *STAT3*-dependent manner. (A) A *MIR506* binding site was predicted in the 3'-UTR of *STAT3* by TargetScan. (B) A luciferase reporter assay showed that *MIR506* directly targeted the *STAT3* 3'-UTR. MDA-PATC53 cells were cotransfected with wild-type or mutant *STAT3* 3'-UTR-luciferase reporter and MIRctrl or *MIR506* mimic for 72 h before analysis. The *firefly* and *renilla* luciferase activities were measured using a Dual Luciferase Reporter Assay System. (C-D) MDA-PATC53, MDA-PATC124, MDA-PATC148, MDA-PATC50, and MDA-PATC69 cells were transfected with MIRctrl or *MIR506*. Whole-cell extracts were subjected to immunoblotting with anti-*STAT3*, anti-p-*STAT3*, and anti-LC3 antibodies. (E) The expression level of *STAT3* was detected by qRT-PCR and normalized to the endogenous control *GAPDH*. (F) Cell death was quantified by trypan blue exclusion assay. Data represent the mean \pm SD of at least 3 independent experiments. NS, not significant; ** $P < 0.01$.

process and modulates autophagy via both transcription-dependent and transcription-independent pathways. Immunoblotting analysis for STAT3-regulated autophagy-related genes revealed a dramatic increase in *BECN1* and decrease in *BCL2* after *MIR506* transfection in PDAC cells (Fig. 6A). Because *BECN1* is essential for autophagy upregulation in response to stress and *BCL2* is a central inhibitor of this process by directly binding *BECN1* via its BH3 domain, we hypothesized that *MIR506* induces autophagy-related cell death through the *STAT3-BCL2-BECN1* signaling pathway.

To confirm that autophagy-related cell death triggered by *MIR506* was mediated by repression of *STAT3* in PDAC cells, gain-of-function and loss-of-function studies were carried out. First, we treated PDAC cells with a selective *STAT3* inhibitor, Stattic, which inhibits activation, dimerization, and nuclear translocation of *STAT3* by interacting with the SH2 domain to imitate the suppressive effect of *MIR506*. Following the decline of phosphorylated *STAT3* (p-*STAT3*; Y705) expression,

BECN1 increased and *BCL2* decreased in both dose-dependent and time-dependent manners in total proteins isolated from the treated cells. The LC3 conversion and AO staining showed dramatic enhancement of autophagic flux (Fig. 6B, C, and S8). The trypan blue exclusion assay also revealed a gradual increase of cell death (Fig. 6D and E). Silencing of *STAT3* by small-interfering RNA (siRNA) knockdown (si-*STAT3*-1 and si-*STAT3*-2), similar to *MIR506*, significantly increased autophagic flux and cell death (Fig. 6F, G and S9).

To determine whether ectopic expression of *STAT3* could rescue the effects of *MIR506*, we established MDA-PATC53 cells that stably overexpressed wild-type or Y705-mutant *STAT3* and subsequently transfected them with *MIR506*. Overexpression of wild-type *STAT3* partially abrogated the *MIR506*-induced downregulation of both total *STAT3* and p-*STAT3*, while overexpression of mutated *STAT3* rescued only the downregulation of total *STAT3*. The forced expression of wild-type *STAT3* significantly counteracted the autophagic flux and

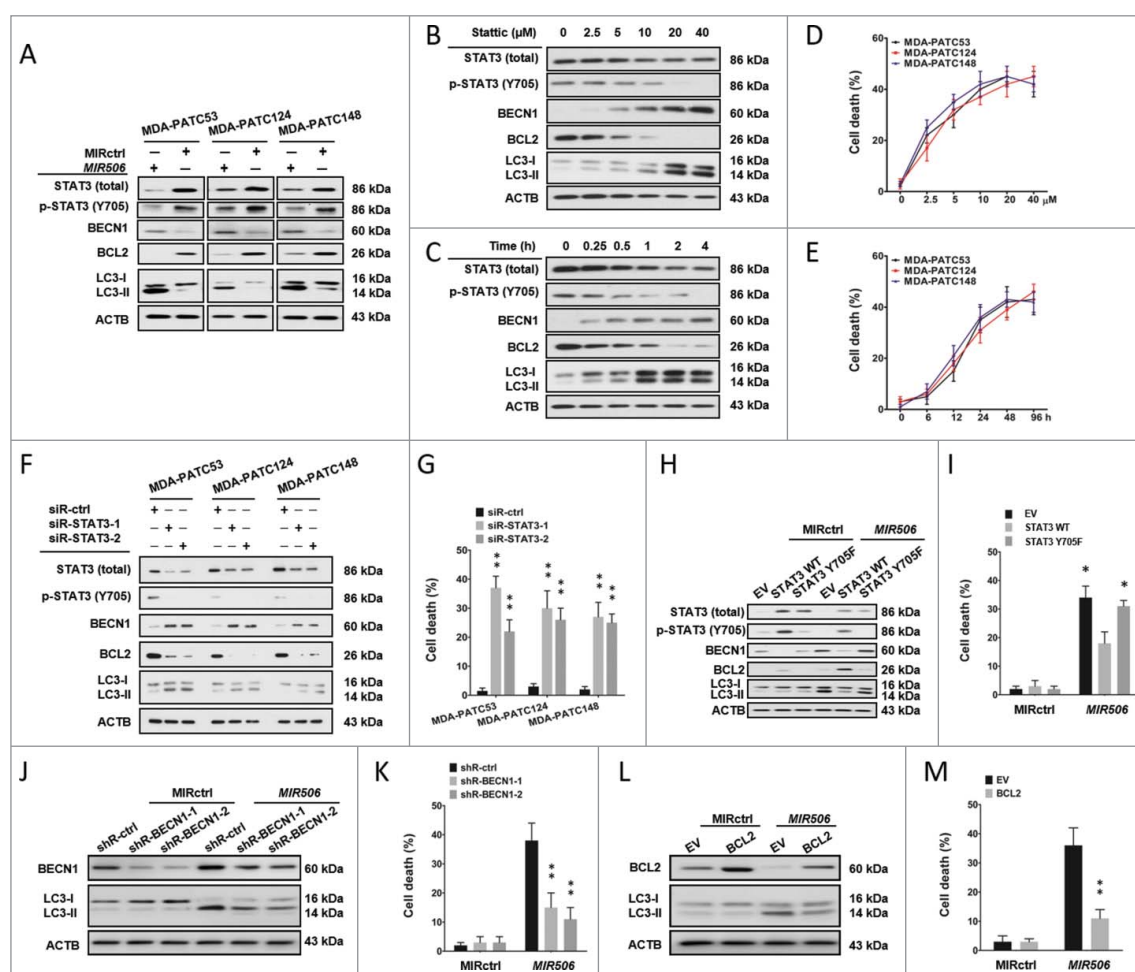


Figure 6. *MIR506* induces autophagy-related cell death through the *STAT3* signaling pathway. (A) MDA-PATC53, MDA-PATC124, and MDA-PATC148 cells were transfected with MIRctrl or *MIR506* for 72 h. Whole-cell extracts were subjected to immunoblotting with anti-*STAT3*, anti-p-*STAT3*, anti-*BECN1*, -*BCL2*, and -*LC3* antibodies. (B-C) MDA-PATC53, MDA-PATC124, and MDA-PATC148 cells were treated with the indicated concentrations of the *STAT3* inhibitor Stattic for the indicated times. (D-E) Cell death was quantified by trypan blue exclusion assay. (F) MDA-PATC53, MDA-PATC124, and MDA-PATC148 cells were transfected with control siRNA (siR-ctrl) or 1 of 2 siRNAs against *STAT3* (siR-*STAT3*-1 or siR-*STAT3*-2). Whole-cell extracts were subjected to immunoblotting with anti-*STAT3*, anti-p-*STAT3*, anti-*BECN1*, -*BCL2*, and -*LC3* antibodies. (G) Cell death was quantified by trypan blue exclusion assay. (H-I) MDA-PATC53 cells overexpressing wild-type or Y705-mutant *STAT3* were transfected with MIRctrl or *MIR506* and analyzed by immunoblotting and trypan blue exclusion assay as described above. (J-K) MDA-PATC53 cells were transfected with control shRNA (shR-ctrl) or 1 of 2 shRNAs against *BECN1* (siR-*BECN1*-1 or siR-*BECN1*-2) and analyzed by immunoblotting and trypan blue exclusion assay as described above. (L-M) MDA-PATC53 cells overexpressing *BCL2* were transfected with MIRctrl or *MIR506* and analyzed by immunoblotting and trypan blue exclusion assay as described above. Data represent the mean \pm SD of at least of 3 independent experiments. NS, not significant; * $P < 0.05$; ** $P < 0.01$.

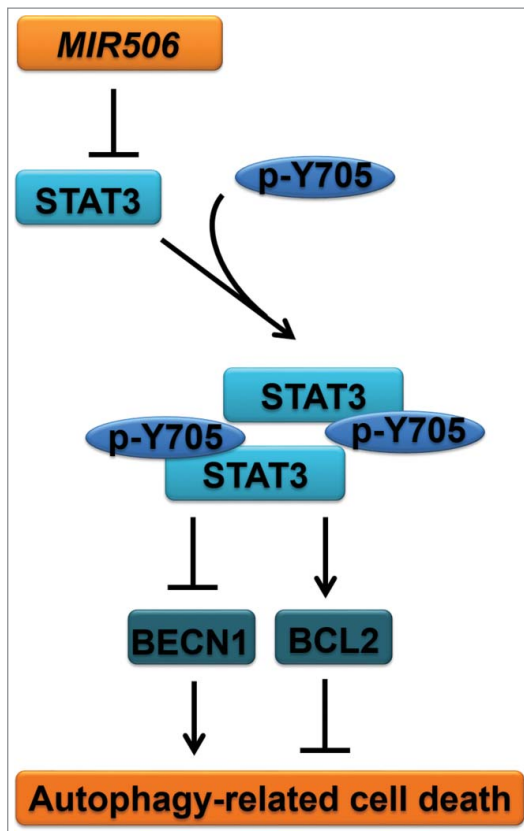


Figure 7. Schematic of the proposed mechanism of *MIR506* induction of autophagy-related cell death in PDAC cells through the *STAT3* signaling pathway.

cell death triggered by *MIR506*, suggesting that *STAT3* mediated the autophagy-related cell death-inducing function of *MIR506* in PDAC (Fig. 6H, I and S10).

To further confirm the major role of *BECN1* and *BCL2* in autophagy-related cell death induced by *MIR506*, we first silenced *BECN1* by siRNA (si-*BECN1*-1 and si-*BECN1*-2) in MDA-PATC53. Western blot showed that knockdown of *BECN1* abrogated the conversion of LC3 caused by *MIR506* (Fig. 6J). Knockdown of *BECN1* also reduced the AO-positive cell ratio and cell death caused by *MIR506* (Fig. 6K and S11). Next, we overexpressed *BCL2* by transfecting MDA-PATC53 cells with a *BCL2* expression plasmid. Overexpression of *BCL2* inhibited the conversion of LC3, reduced the AO-positive cell ratio (Fig. 6L and S12) and rescued the cell death caused by *MIR506* (Fig. 6L).

Together, these results suggest that *MIR506*-mediated regulation of the *STAT3*-*BCL2*-*BECN1* signaling pathway is one of the major mechanisms underlying induction of autophagy-related cell death. The proposed mechanism is summarized in Figure 7.

Discussion

In this study, we showed that decreased expression of *MIR506* accompanied disease progression in human PDAC. The normal pancreatic tissue is a mixture of acinar, ductal and endocrine tissue. The relative contributions of each component may vary in different samples, which may explain the heterogeneity observed in normal tissues. Future studies are needed to discern

the relative expression levels of *MIR506* in different cell components in normal pancreas and understand its role in cellular differentiation. The most important contribution of this study to the understanding of *MIR506* as a tumor suppressor is that we showed for the first time that *MIR506* triggered autophagic flux and autophagy-related cell death in PDAC cells. We further demonstrated that *MIR506* regulated autophagy-related cell death through direct targeting of *STAT3*. Silencing and inhibiting *STAT3* recapitulated the effects of *MIR506*, whereas forced expression of wild-type *STAT3*, but not the kinase-inactive mutant form, abrogated the effects of *MIR506*. The regulatory effect of *MIR506* on *STAT3* led to inhibition of *BCL2* and activation of *BECN1*. These findings demonstrate that autophagy-related cell death is an unrecognized mechanism underlying the anticancer effects of *MIR506* against human PDAC cells.

Autophagy is an evolutionarily conserved process that recycles nonessential cytosolic materials for degradation by lysosomes to maintain cellular homeostasis and overcome metabolic stress and nutrient deprivation.³⁶⁻³⁷ The roles of autophagy in PDAC are divergent and the molecular mechanisms have not been fully explained.³⁸ In PDAC cells, autophagy usually functions as a cytoprotective strategy in response to hypoxic and acidic microenvironments with starved and stressful metabolic conditions.³⁹⁻⁴⁴ Fujii et al. first revealed that high LC3 expression levels were significantly correlated with poor outcome and shorter disease-free intervals in PDAC.⁴⁵ Yang et al. demonstrated that the growth of PDAC had a distinct dependence on autophagy in vivo and in vitro.⁴⁶ Although autophagy often contributes to therapeutic resistance, excessive or prolonged autophagy causes autophagy-related cell death as a tumor-suppressive mechanism in response to some treatments, leading to tumor regression.⁴⁷ Gemcitabine, a standard chemotherapeutic agent for the treatment of PDAC, induces autophagy-related cell death by activating the expression of *VMP1*, which could trigger autophagy by interacting with *BECN1*.⁴⁸ Capecitabine induces excessive autophagy that leads to autophagy-related cell death by inhibiting SRC kinase, which plays a role in regulating autophagy.⁴⁹ Cannabinoids show a synergistic effect with gemcitabine in inhibiting cell growth by inducing reactive oxygen species-mediated autophagy-related cell death that sensitizes chemoresistant cells to gemcitabine.⁵⁰ Proton pump inhibitors show antiproliferative activities in cancer therapy by inhibiting the vacuolar ATPase, which plays a crucial role in tumorigenesis. In PDAC, omeprazole modulated chemoresistance and induced tumor cell death directly by enhancing autophagic activity in combination with either gemcitabine or 5-FU.⁵¹

BCL2 is a crucial regulator of PCD by preventing cells from undergoing apoptosis. Overexpression of *BCL2* contributes to the development of resistance to chemotherapy, radiation, and hormone therapy. Recent evidence indicates that *BCL2* is also involved in regulation of autophagy-related cell death (type II PCD). *BCL2* inhibits induction of autophagy by binding and blocking *BECN1*, a central autophagy-promoting tumor suppressor. Therapeutic targeting of *BCL2* in cancer cells with *BCL2* overexpression-induced chemoresistance, either by small molecule inhibitors or antisense methodology, is emerging as an effective anticancer strategy. Along these lines, silencing of *BCL2* induces autophagy-related cell death in *BCL2*-

overexpressing breast cancer cells. In human leukemic cells, downregulation of *BCL2* triggers autophagy-related cell death.⁵² Sorafenib induces cell death in vitro and suppresses tumor growth in vivo through an autophagy-dependent mechanism mediated by *BECN1* in hepatocellular carcinoma.⁵³ Overexpression of *BCL2* is common in PDAC and results in an extreme resistance to apoptotic PCD. In the present study, *MIR506* showed a prominent autophagy-related cell death-inducing function mediated through the *STAT3-BCL2-BECN1* pathway.

Taken together, our findings provide evidence that *MIR506* triggered autophagy-related cell death in human PDAC cells and that this function was mediated through downregulation of *STAT3*, which in turn inhibited *BCL2* and promoted *BECN1* function. These results provided a mechanistic characterization of *MIR506*-induced autophagy-related cell death and suggest that further exploration of this approach, as a potentially effective therapeutic option against human PDAC, is warranted.

Materials and methods

Clinical specimens

Paired human PDAC and adjacent nontumor pancreatic tissues were collected from archived surgical specimens from 92 patients with biopsy-proven PDAC who underwent operation at Tianjin Medical University General Hospital between 2009 and 2013. Samples were immediately snap-frozen in liquid nitrogen and stored in liquid nitrogen until RNA extraction. Each patient's clinical and biological information was registered and follow-up data were recorded after informed consent was obtained. This study was approved by the institutional research ethics committee at Tianjin Medical University General Hospital. The patients' demographic and clinical characteristics are summarized in Table S1.

Patient-derived xenograft cell lines and cell culture

Human PDAC PDX cell lines MDA-PATC50, MDA-PATC53, MDA-PATC69, MDA-PATC124, and MDA-PATC148 were established as previously reported and cultured in Dulbecco modified essential/F12 50:50 medium supplemented with 10% fetal bovine serum in an incubator with 5% CO₂ atmosphere at 37°C.⁵⁴

RNA isolation and qRT-PCR

The total RNA, including miRNA, was extracted from cells and tissues by using the mirVana Isolation Kit (Ambion, AM1560). Reverse-transcription was performed by using TaqMan miRNA Reverse Transcription kit (Applied Biosystems, 4366596) or SuperScript II Reverse Transcriptase (Invitrogen, 18064014). TaqMan MicroRNA Assay and TaqMan Gene Expression Assays (Applied Biosciences, A25576 and 4331182, respectively) were used to detect and quantify *MIR506* and *STAT3*. Relative expression was normalized to the endogenous control *GAPDH* or *RNU6* using the 2^{-ΔΔCt} method. Experiments were carried out in triplicate.

Reagents and antibodies

The following antibodies were used: anti-LGALS1 (Abcam, ab25138) 1:1,000; anti-LGALS3 (Abcam, ab53082) 1:1,000; anti-LC3 (Cell Signaling Technology, 3868) 1:500; anti-STAT3 (Cell Signaling Technology, 12640) 1:500; anti-phospho-STAT3 (Tyr705; Cell Signaling Technology, 9145) 1:250; anti-CASP3/caspase-3 (Santa Cruz Biotechnology, sc-7148) 1:500; anti-CASP9/caspase-9 (Santa Cruz Biotechnology, sc-70505) 1:500; anti-BECN1/Beclin-1 (Santa Cruz Biotechnology, sc-11427) 1:500; anti-BCL2/Bcl-2 (Santa Cruz Biotechnology, sc-7382) 1:250; anti-SQSTM1 (Santa Cruz Biotechnology, sc-28359) 1:500; and anti-ACTB/ β -Actin (Santa Cruz Biotechnology, sc-47778) 1:1,000. See Table S2 for a complete list of antibodies used. Other chemicals used included IM-54 (Sigma, SML0412), 5-FU (Sigma, 03738), z-VAD-FMK (Sigma, V116), t-BHP (Sigma, 416665), 3-MA (Sigma, M9281), AO (Sigma, A8097), Baf-A (Sigma, B1793), Stattic (Sigma, S7947), CQ (Sigma, C6628), and LLOMe (Santa Cruz Biotechnology, sc-285992).

Transfection

To generate the Y705-mutated *STAT3* sequence, nucleotide sequences coding amino acid residues Y705 of *STAT3* were mutated to F705 using the QuikChange Lightning site-directed mutagenesis kit (Agilent Technologies, 210519). Introduction of the mutation was verified by sequencing. Human wild-type *BCL2*, and wild-type and mutated *STAT3* cDNAs were cloned into the pcDNA3.1 plasmid (Invitrogen, V79020) and verified by sequencing. ShRNA plasmids for *BECN1* (TRCN0000299789 and TRCN0000299790), *ATG5* (TRCN0000151474 and TRCN0000330392), and *ATG7* (TRCN0000007586 and TRCN0000007587) were purchased from Sigma. Cells were transfected with 4 μ g of plasmids by FuGENE HD (Promega, E2311) for 48 h, followed by G418 selection for 3 wk.

The miRNA mimics of *MIR506* and control miRNA (MIRctrl) were purchased from Dharmacon (c-300846-05 and CN-001000-01). siRNAs for *STAT3* (SASI_Hs01_00121206 and 00121207) were obtained from Sigma. Cells were seeded in 6-well plates at 2 \times 10⁵/well and allowed to attach overnight. They were then transfected with *MIR506* mimic, MIRctrl, or siRNA for *STAT3* by using Lipofectamine RNAiMAX (Invitrogen, 13778150). Total RNA and protein were collected 48 h after transfection.

Luciferase reporter assay

The 3'-UTR sequences of *STAT3* containing the wild-type or mutant predicted binding site of *MIR506* were cloned into the pGL3 vector (Promega, E1751). MDA-PATC53 cells transfected with MIRctrl or *MIR506* mimic were seeded and cotransfected with pGL3 and pRL-TK vector (Promega, E1751 and E2241) using FuGENE HD. The *firefly* and *renilla* luciferase activities were measured using a Dual Luciferase Reporter Assay System according to the manufacturer's protocol (Promega, E1910).

Cell viability assay

Cell viability was assessed by MTT assay. MIRctrl- or *MIR506*-transfected cells were seeded into 96-well plates and incubated for 24, 48, 72, 96, or 120 h at 37°C. MTT (Sigma, M2128) was added to each well at a final concentration of 5 mg/L and incubated for a further 4 h. After removal of the medium, 150 μ L of dimethyl sulfoxide (DMSO) was added to each well to dissolve the crystal formazan dye. The absorbance at a wavelength of 540 nm (A540) was determined for each well using a microplate reader.

Cell death assay

Cell death was first quantified by trypan blue exclusion assay. Both floating and adherent cells were trypsinized, collected, and resuspended in 1 mL of phosphate-buffered saline solution (PBS; Gibco, 10010023). Cell death was determined as the percentage of stained cells (blue) over the total cells. Cell death was also assessed by using the Apoptosis Detection Kit (BD Pharmingen, 556547). The treated cells were incubated with fluorescein isothiocyanate (FITC)-conjugated anti-ANXA5 antibody and PI in binding buffer and analyzed by flow cytometry.

Apo-BrdU apoptosis assays

Cell apoptosis was assessed with an Apo-BrdU kit (BD Pharmingen, 556405). Cells were fixed and treated with terminal deoxynucleotidyl transferase to catalyze an addition of BrdUTP to the 3'-hydroxyl termini of fragmented DNA, which were then stained with FITC-conjugated anti-BrdU antibody. DNA break sites were identified and analyzed by flow cytometry to determine apoptotic fractions.

Western blotting

Cells were harvested and subjected to lysis in RIPA Buffer (Thermo Fisher Scientific, 89901) with 1:100 Halt Phosphatase Inhibitor Cocktail (Thermo Fisher Scientific, 78426). The whole-cell lysate from each sample was separated by electrophoresis on a 10% polyacrylamide gel. The membrane was blocked in 5% nonfat milk in Tris Buffered Saline (TBS; BIO-RAD, 1706435, pH7.6) with 0.1% Tween-20 (Sigma, P2287) and incubated with primary antibodies at 4°C overnight. The secondary antibodies (Santa Cruz Biotechnology, sc-2077 or sc-2375) were used at a concentration of 1:10,000. The proteins were visualized using the SuperSignal West Pico chemiluminescent substrate or Femto Maximum Sensitivity Substrate (Thermo Fisher Scientific, 34080 or 34095).

Immunofluorescence microscopy imaging

Cells were seeded into Lab-Tek II Chamber Slides (Thermo Fisher Scientific, 154526) and cultured in complete medium. After treatment, cells were fixed for 15 min with 4% paraformaldehyde, permeated and blocked in blocking solution (1 \times PBS with 10% normal goat serum (Sigma, G9023) and 0.5% NP40 (Abcam, ab142227) for 4 h, and incubated with anti-

human LC3 antibody (1:500 dilution), anti-human LGALS1 (1:1,000 dilution), or anti-human LGALS3 (1:1,000 dilution) at 4°C overnight and then with Alexa Fluor 488 goat anti-rabbit IgG (Invitrogen, A-11034) at 1:1,000 dilution at ambient temperature for 1 h. Nuclei were counterstained with 4',6-diamidino-2-phenylindole (DAPI; Thermo Fisher Scientific, P36931). The fluorescence images were captured with a ZEISS Axioplan 2 microscope.

Autophagic flux measurement

Autophagic flux was measured in cells transfected with Autophagy Tandem Sensor RFP-GFP-LC3 (Life Technologies, P36239). After 24 h, the fluorescence images were captured using a ZEISS Axioplan 2 microscope and the autophagosomes (yellow dots) and autolysosomes (only red dots) were counted.

Acridine orange staining

After treatment, the cells were incubated with 1 mg/mL AO solution (Sigma, A8097) for 15 min in complete medium. The cells were then collected and analyzed by flow cytometry. In AO-stained cells, the acidic compartments (autolysosomes) appeared red. The intensity of the red fluorescence indicated the degree of autophagy.

Statistical analysis

Data are expressed as the mean \pm SD of at least 3 separate experiments performed in triplicate. A Student *t* test was performed to compare the differences between groups. *P* values < 0.05 were considered statistically significant. Statistically significant differences are indicated in figures by asterisks (**P* < 0.05, ***P* < 0.01). SPSS 17.0 software (SPSS Inc., Chicago, IL) was used for all statistical analyses.

Abbreviations

3-MA	3-methyladenine
5-FU	5-fluorouracil
AO	acridine orange
ATG5	autophagy-related 5
ATG7	autophagy-related 7
Baf-A	bafilomycin A ₁
BCL2	BCL2, apoptosis regulator
BECN1	Beclin 1
BrdU	bromodeoxyuridine
CASP3	caspase 3
CASP9	caspase 9
CQ	chloroquine
DAPI	4',6-diamidino-2-phenylindole
FITC	fluorescein isothiocyanate
IM-54	2-(1H-Indol-3-yl)-3-pentylamino-maleimide
LLOME	L-leucyl-L-leucine methyl ester
LMP	lysosomal membrane permeabilization
MTT	3-(4,5-dimethylthiazol-2-yl)-2,5-diphenyltetrazolium bromide
PBS	phosphate-buffered saline
PCD	programmed cell death

PDAC	pancreatic ductal adenocarcinoma
PDX	patient-derived xenograft
PI	propidium iodide
qRT-PCR	quantitative reverse-transcriptase polymerase chain reaction
shRNA	short-hairpin RNA
siRNA	small-interfering RNA
SQSTM1	sequestosome 1
STAT3	signal transducer and activator of transcription 3
t-BHP	tert-butyl hydroperoxide
z-VAD-FMK	N-benzyloxycarbonyl-Val-Ala-Asp-fluoro-methyl ketone

Disclosure of potential conflicts of interest

The authors have no potential conflicts of interest to disclose.

Acknowledgments

We thank Kathryn L. Hale, Department of Scientific Publications at The University of Texas MD Anderson Cancer Center, for editing this manuscript. We thank Drs. Gregory A. Hawkins, Peiqing Sun, and Peter A. Antinozzi for valuable discussion on the results and figures.

Funding

This study was partially supported by the U.S. National Institutes of Health/National Cancer Institute under awards P30CA016672 to MD Anderson Cancer Center and P30CA012197 to Wake Forest Baptist Comprehensive Cancer Center. This work was also supported by a grant from the National Foundation for Cancer Research (to W.Z.) and the Skip Viragh Family Foundation (to J.F.). W.Z. was supported by the Hanes and Willis Family Endowed Professorship in Cancer. L.S. was supported by a Postdoctoral Fellowship from the Tianjin Medical University General Hospital and Comprehensive Cancer Center of Wake Forest Baptist Medical Center.

References

- [1] Ryan DP, Hong TS, Bardeesy N. Pancreatic adenocarcinoma. *N Engl J Med* 2014; 371:1039-49; PMID:25207767; <http://dx.doi.org/10.1056/NEJMra1404198>
- [2] Siegel RL, Miller KD, Jemal A. Cancer statistics, 2015. *CA Cancer J Clin* 2015; 65:5-29; <http://dx.doi.org/10.3322/caac.21254>
- [3] Neoptolemos JP. Adjuvant treatment of pancreatic cancer. *Eur J Cancer* 2011; 47 Suppl 3:S378-80; PMID:21944022; [http://dx.doi.org/10.1016/S0959-8049\(11\)70210-6](http://dx.doi.org/10.1016/S0959-8049(11)70210-6)
- [4] Barugola G, Partelli S, Marcucci S, Sartori N, Capelli P, Bassi C, Pedrazoli P, Falconi M. Resectable pancreatic cancer: who really benefits from resection? *Ann Surg Oncol* 2009; 16:3316-22; PMID:19707831; <http://dx.doi.org/10.1245/s10434-009-0670-7>
- [5] Conroy T, Desseigne F, Ychou M, Bouché O, Guimbaud R, Bécouarn Y, Adenis A, Raoul JL, Gourgou-Bourgade S, de la Fouchardière C, et al. FOLFIRINOX versus gemcitabine for metastatic pancreatic cancer. *N Engl J Med* 2011; 364:1817-25; PMID:21561347; <http://dx.doi.org/10.1056/NEJMoa1011923>
- [6] Hale AN, Ledbetter DJ, Gawriluk TR, Rucker EB 3rd. Autophagy: regulation and role in development. *Autophagy* 2013; 9:951-72; PMID:24121596; <http://dx.doi.org/10.4161/autophagy.24273>
- [7] Rabinowitz JD, White E. Autophagy and metabolism. *Science* 2010; 330:1344-8; PMID:21127245; <http://dx.doi.org/10.1126/science.1193497>
- [8] Ito H, Aoki H, Kühnel F, Kondo Y, Kubicka S, Wirth T, Iwado E, Iwamaru A, Fujiwara K, Hess KR, et al. Autophagic cell death of malignant glioma cells induced by a conditionally replicating adenovirus. *J Natl Cancer Inst* 2006; 98:625-36; PMID:16670388; <http://dx.doi.org/10.1093/jnci/djj161>
- [9] Yu L, Alva A, Su H, Dutt P, Freundt E, Welsh S, Baehrecke EH, Lenardo MJ. Regulation of an ATG7-beclin 1 program of autophagic cell death by caspase-8. *Science* 2004; 304:1500-2; PMID:15131264; <http://dx.doi.org/10.1126/science.1096645>
- [10] Kroemer G, Levine B. Autophagic cell death: the story of a misnomer. *Nat Rev Mol Cell Biol* 2008; 9:1004-10; PMID:18971948; <http://dx.doi.org/10.1038/nrm2529>
- [11] Berry DL, Baehrecke EH. Autophagy functions in programmed cell death. *Autophagy* 2008; 4:359-60; PMID:18212526; <http://dx.doi.org/10.4161/autophagy.5575>
- [12] Pattingre S, Tassa A, Qu X, Garuti R, Liang XH, Mizushima N, Packer M, Schneider MD, Levine B. Bcl-2 antiapoptotic proteins inhibit Beclin 1-dependent autophagy. *Cell* 2005; 122:927-39; PMID:16179260; <http://dx.doi.org/10.1016/j.cell.2005.07.002>
- [13] Akar U, Chaves-Reyez A, Barria M, Tari A, Sanguino A, Kondo Y, Kondo S, Arun B, Lopez-Berestein G, Ozpolat B. Silencing of Bcl-2 expression by small interfering RNA induces autophagic cell death in MCF-7 breast cancer cells. *Autophagy* 2008; 4:669-79; PMID:18424910; <http://dx.doi.org/10.4161/autophagy.6083>
- [14] Shimizu S, Kanaseki T, Mizushima N, Mizuta T, Arakawa-Kobayashi S, Thompson CB, Tsujimoto Y. Role of Bcl-2 family proteins in a non-apoptotic programmed cell death dependent on autophagy genes. *Nat Cell Biol* 2004; 6:1221-8; PMID:15558033; <http://dx.doi.org/10.1038/ncb1192>
- [15] Yang A, Rajeshkumar NV, Wang X, Yabuuchi S, Alexander BM, Chu GC, Von Hoff DD, Maitra A, Kimmelman AC. Autophagy is critical for pancreatic tumor growth and progression in tumors with p53 alterations. *Cancer Discov* 2014; 4:905-13; PMID:24875860; <http://dx.doi.org/10.1158/2159-8290.CD-14-0362>
- [16] Yang J, Chatterjee-Kishore M, Staugaitis SM, Nguyen H, Schlessinger K, Levy DE, Stark GR. Novel roles of unphosphorylated STAT3 in oncogenesis and transcriptional regulation. *Cancer Res* 2005; 65:939-47; PMID:15705894
- [17] Kang R, Tang D, Lotze MT, Zeh HJ 3rd. AGER/RAGE-mediated autophagy promotes pancreatic tumorigenesis and bioenergetics through the IL6-pSTAT3 pathway. *Autophagy* 2012; 8:989-91; PMID:22722139; <http://dx.doi.org/10.4161/autophagy.20258>
- [18] Gong J, Muñoz AR, Chan D, Ghosh R, Kumar AP. STAT3 down regulates LC3 to inhibit autophagy and pancreatic cancer cell growth. *Oncotarget* 2014; 5:2529-41; PMID:24796733; <http://dx.doi.org/10.18632/oncotarget.1810>
- [19] Niso-Santano M, Shen S, Adjemian S, Malik SA, Mariño G, Lachkar S, Senovilla L, Kepp O, Galluzzi L, Maiuri MC, et al. Direct interaction between STAT3 and EIF2AK2 controls fatty acid-induced autophagy. *Autophagy* 2013; 9:415-7; PMID:23221979; <http://dx.doi.org/10.4161/autophagy.22910>
- [20] Huang YH, Yang PM, Chuah QY, Lee YJ, Hsieh YF, Peng CW, Chiu SJ. Autophagy promotes radiation-induced senescence but inhibits bystander effects in human breast cancer cells. *Autophagy* 2014; 10:1212-28; PMID:24813621; <http://dx.doi.org/10.4161/autophagy.28772>
- [21] Maycotte P, Gearheart CM, Barnard R, Aryal S, Mulcahy Levy JM, Fosmire SP, Hansen RJ, Morgan MJ, Porter CC, Gustafson DL, et al. STAT3-mediated autophagy dependence identifies subtypes of breast cancer where autophagy inhibition can be efficacious. *Cancer Res* 2014; 74:2579-90; PMID:24590058; <http://dx.doi.org/10.1158/0008-5472.CAN-13-3470>
- [22] Yokoyama T, Kondo Y, Kondo S. Roles of mTOR and STAT3 in autophagy induced by telomere 3' overhang-specific DNA oligonucleotides. *Autophagy* 2007; 3:496-8; PMID:17617738; <http://dx.doi.org/10.4161/autophagy.4602>
- [23] Yoon S, Woo SU, Kang JH, Kim K, Kwon MH, Park S, Shin HJ, Gwak HS, Chwa YJ. STAT3 transcriptional factor activated by reactive oxygen species induces IL6 in starvation-induced autophagy of cancer cells. *Autophagy* 2010; 6:1125-38; PMID:20930550; <http://dx.doi.org/10.4161/autophagy.6.8.13547>
- [24] Noman MZ, Janji B, Kaminska B, Van Moer K, Pierson S, Przanowski P, Buart S, Berchem G, Romero P, Mami-Chouaib F, et al.

- Blocking hypoxia-induced autophagy in tumors restores cytotoxic T-cell activity and promotes regression. *Cancer Res* 2011; 71:5976-86; PMID:21810913; <http://dx.doi.org/10.1158/0008-5472.CAN-11-1094>
- [25] Zhang T, Li Y, Park KA, Byun HS, Won M, Jeon J, Lee Y, Seok JH, Choi SW, Lee SH, et al. Cucurbitacin induces autophagy through mitochondrial ROS production which counteracts to limit caspase-dependent apoptosis. *Autophagy* 2012; 8:559-76; PMID:22441021; <http://dx.doi.org/10.4161/auto.18867>
- [26] Yang D, Sun Y, Hu L, Zheng H, Ji P, Pecot CV, Zhao Y, Reynolds S, Cheng H, Rupaimoole R, et al. Integrated analyses identify a master microRNA regulatory network for the mesenchymal subtype in serous ovarian cancer. *Cancer Cell* 2013; 23:186-99; PMID:23410973; <http://dx.doi.org/10.1016/j.ccr.2012.12.020>
- [27] Sun Y, Hu L, Zheng H, Bagnoli M, Guo Y, Rupaimoole R, Rodriguez-Aguayo C, Lopez-Berestein G, Ji P, Chen K, et al. MiR-506 inhibits multiple targets in the epithelial-to-mesenchymal transition network and is associated with good prognosis in epithelial ovarian cancer. *J Pathol* 2015; 235:25-36; PMID:25230372; <http://dx.doi.org/10.1002/path.4443>
- [28] Liu G, Sun Y, Ji P, Li X, Cogdell D, Yang D, Parker Kerrigan BC, Shmulevich I, Chen K, Sood AK, et al. MiR-506 suppresses proliferation and induces senescence by directly targeting the CDK4/6-FOXMI axis in ovarian cancer. *J Pathol* 2014; 233:308-18; PMID:24604117; <http://dx.doi.org/10.1002/path.4348>
- [29] Wen SY, Lin Y, Yu YQ, Cao SJ, Zhang R, Yang XM, Li J, Zhang YL, Wang YH, Ma MZ, et al. miR-506 acts as a tumor suppressor by directly targeting the hedgehog pathway transcription factor Gli3 in human cervical cancer. *Oncogene* 2015; 34:717-25; PMID:24608427; <http://dx.doi.org/10.1038/ncr.2014.9>
- [30] Liu G, Yang D, Rupaimoole R, Pecot CV, Sun Y, Mangala LS, Li X, Ji P, Cogdell D, Hu L, et al. Augmentation of response to chemotherapy by microRNA-506 through regulation of RAD51 in serous ovarian cancers. *J Natl Cancer Inst* 2015; 107:djv108; PMID:25995442; <http://dx.doi.org/10.1093/jnci/djv108>
- [31] Li J, Wu H, Li W, Yin L, Guo S, Xu X, Ouyang Y, Zhao Z, Liu S, Tian Y, et al. Downregulated miR-506 expression facilitates pancreatic cancer progression and chemoresistance via SPHK1/Akt/NF- κ B signaling. *Oncogene* 2016; 35(42):5501-5514. [Epub ahead of print]; PMID:27065335; <http://dx.doi.org/10.1038/ncr.2016.90>
- [32] Du J, Zheng X, Cai S, Zhu Z, Tan J, Hu B, Huang Z, Jiao H. MicroRNA-506 participates in pancreatic cancer pathogenesis by targeting PIM3. *Mol Med Rep* 2015; 12:5121-6; PMID:26238203
- [33] Peng T, Zhou L, Zuo L, Luan Y. miR-506 functions as a tumor suppressor in glioma by targeting STAT3. *Oncol Rep* 2016; 35:1057-64; PMID:26554866
- [34] Aits S, Krickler J, Liu B, Ellegaard AM, Hämälistö S, Tvingsholm S, Corcelle-Termeau E, Høgh S, Farkas T, Holm Jonassen A, et al. Sensitive detection of lysosomal membrane permeabilization by lysosomal galectin puncta assay. *Autophagy* 2015; 11:1408-24; PMID:26114578; <http://dx.doi.org/10.1080/15548627.2015.1063871>
- [35] Klionsky DJ, Abdelmohsen K, Abe A, Abedin MJ, Abeliovich H, Acevedo Arozana A, Adachi H, Adams CM, Adams PD, Adeli K, et al. Guidelines for the use and interpretation of assays for monitoring autophagy (3rd edition). *Autophagy* 2016; 12:1-222; PMID:26799652; <http://dx.doi.org/10.1080/15548627.2015.1100356>
- [36] Mathew R, Karantza-Wadsworth V, White E. Role of autophagy in cancer. *Nat Rev Cancer* 2007; 7:961-7; PMID:17972889; <http://dx.doi.org/10.1038/nrc2254>
- [37] Høyer-Hansen M, Jäättelä M. Autophagy: an emerging target for cancer therapy. *Autophagy* 2008; 4:574-80; PMID:18362515; <http://dx.doi.org/10.4161/auto.5921>
- [38] Neesse A, Michl P, Frese KK, Feig C, Cook N, Jacobetz MA, Lolkema MP, Buchholz M, Olive KP, Gress TM, et al. Stromal biology and therapy in pancreatic cancer. *Gut* 2011; 60:861-8; PMID:20966025; <http://dx.doi.org/10.1136/gut.2010.226092>
- [39] Noman MZ, Janji B, Berchem G, Mami-Chouaib F, Chouaib S. Hypoxia-induced autophagy: a new player in cancer immunotherapy? *Autophagy* 2012; 8:704-6; PMID:22441015; <http://dx.doi.org/10.4161/auto.19572>
- [40] Azad MB, Chen Y, Henson ES, Cizeau J, McMillan-Ward E, Israels SJ, Gibson SB. Hypoxia induces autophagic cell death in apoptosis-competent cells through a mechanism involving BNIP3. *Autophagy* 2008; 4:195-204; PMID:18059169; <http://dx.doi.org/10.4161/auto.5278>
- [41] Farrall AL, Whitelaw ML. The HIF1 alpha-inducible pro-cell death gene BNIP3 is a novel target of SIM2s repression through cross-talk on the hypoxia response element. *Oncogene* 2009; 28:3671-80; PMID:19668230; <http://dx.doi.org/10.1038/ncr.2009.228>
- [42] Morselli E, Galluzzi L, Kepp O, Mariño G, Michaud M, Vitale I, Maiuri MC, Kroemer G. Oncosuppressive functions of autophagy. *Antioxid Redox Signal* 2011; 14:2251-69; PMID:20712403; <http://dx.doi.org/10.1089/ars.2010.3478>
- [43] Cuervo AM, Macian F. Autophagy, nutrition and immunology. *Mol Aspects Med* 2012; 33:2-13; PMID:21982744; <http://dx.doi.org/10.1016/j.mam.2011.09.001>
- [44] Navarro-Yepes J, Burns M, Anandhan A, Khalimonchuk O, del Razo LM, Quintanilla-Vega B, Pappa A, Panayiotidis MI, Franco R. Oxidative stress, redox signaling, and autophagy: cell death versus survival. *Antioxid Redox Signal* 2014; 21:66-85; PMID:24483238; <http://dx.doi.org/10.1089/ars.2014.5837>
- [45] Fujii S, Mitsunaga S, Yamazaki M, Hasebe T, Ishii G, Kojima M, Kinoshita T, Ueno T, Esumi H, Ochiai A. Autophagy is activated in pancreatic cancer cells and correlates with poor patient outcome. *Cancer Sci* 2008; 99:1813-9; PMID:18616529; <http://dx.doi.org/10.1111/j.1349-7006.2008.00743.x>
- [46] Yang S, Wang X, Contino G, Liesa M, Sahin E, Ying H, Bause A, Li Y, Stommel JM, Dell'antonio G, et al. Pancreatic cancers require autophagy for tumor growth. *Genes Dev* 2011; 25:717-29; PMID:21406549; <http://dx.doi.org/10.1101/gad.2016111>
- [47] Zhang G, Park MA, Mitchell C, Hamed H, Rahmani M, Martin AP, Curiel DT, Yacoub A, Graf M, Lee R, et al. Vorinostat and sorafenib synergistically kill tumor cells via FLP1 suppression and CD95 activation. *Clin Cancer Res* 2008; 14:5385-99; PMID:18765530; <http://dx.doi.org/10.1158/1078-0432.CCR-08-0469>
- [48] Pardo R, Lo Ré A, Archange C, Ropolo A, Papademetrio DL, Gonzalez CD, Alvarez EM, Iovanna JL, Vaccaro MI. Gemcitabine induces the VMP1-mediated autophagy pathway to promote apoptotic death in human pancreatic cancer cells. *Pancreatology* 2010; 10:19-26; PMID:20299819; <http://dx.doi.org/10.1159/000264680>
- [49] Sheikh R, Walsh N, Clynes M, O'Connor R, McDermott R. Challenges of drug resistance in the management of pancreatic cancer. *Expert Rev Anticancer Ther* 2010; 10:1647-61; PMID:20942635; <http://dx.doi.org/10.1586/era.10.148>
- [50] Donadelli M, Dando I, Zaniboni T, Costanzo C, DallaPozza E, Scupoli MT, Scarpa A, Zappavigna S, Marra M, Abbruzzese A, et al. Gemcitabine/cannabinoid combination triggers autophagy in pancreatic cancer cells through a ROS-mediated mechanism. *Cell Death Dis* 2011; 2:e152; PMID:21525939; <http://dx.doi.org/10.1038/cddis.2011.36>
- [51] Udelnow A, Kreyes A, Ellinger S, Landfester K, Walther P, Klapperstueck T, Wohlrab J, Henne-Bruns D, Knippschild U, Würfl P. Omeprazole inhibits proliferation and modulates autophagy in pancreatic cancer cells. *PLoS One* 2011; 6:e20143; PMID:21629657; <http://dx.doi.org/10.1371/journal.pone.0020143>
- [52] Saeki K, Yuo A, Okuma E, Yazaki Y, Susin SA, Kroemer G, Takaku F. Bcl-2 down-regulation causes autophagy in a caspase-independent manner in human leukemic HL60 cells. *Cell Death Differ* 2000; 7:1263-9; PMID:11175264; <http://dx.doi.org/10.1038/sj.cdd.4400759>
- [53] Tai WT, Shiau CW, Chen HL, Liu CY, Lin CS, Cheng AL, Chen PJ, Chen KF. Mcl-1-dependent activation of Beclin 1 mediates autophagic cell death induced by sorafenib and SC-59 in hepatocellular carcinoma cells. *Cell Death Dis* 2013; 4:e485; PMID:23392173; <http://dx.doi.org/10.1038/cddis.2013.18>
- [54] Kang Y, Zhang R, Suzuki R, Li SQ, Roife D, Truty MJ, Chatterjee D, Thomas RM, Cardwell J, Wang Y, et al. Two-dimensional culture of human pancreatic adenocarcinoma cells results in an irreversible transition from epithelial to mesenchymal phenotype. *Lab Invest* 2015; 95:207-22; PMID:25485535; <http://dx.doi.org/10.1038/labinvest.2014.143>